The paper was presented at the Twelfth Meeting
"New Trends in Fatigue and Fracture" (NT2F12)
Brasov, Romania, 27–30 May, 2012

Ivana Atanasovska[1], Dejan Momčilović[2], Meri Burzić[3], Tomaž Vuherer[4]

COUPLED NONLINEAR PROBLEMS IN FINITE ELEMENT ANALYSIS – A CASE STUDY

SPREGNUTI NELINEARNI PROBLEMI U ANALIZI KONAČNIM ELEMENTIMA – STUDIJA SLUČAJA

Originalni naučni rad / Original scientific paper
UDK /UDC: 539.3: 669.14
Paper received: 11.10.2012.

Adresa autora / Author's address:
[1)] Institute Kirilo Savić, Belgrade, Serbia
[2)] Institute for Testing of Materials–IMS, Belgrade, Serbia, dejan.momcilovic@institutims.rs
[3)] University of Belgrade, Faculty of Mechanical Engineering – Innovation Centre, Belgrade, Serbia
[4)] University of Maribor, Faculty of Mechanical Engineering, Maribor, Slovenia

Keywords
- kinetic energy absorber
- railway
- elastic plastic deformation
- contact
- finite element analysis (FEA)

Ključne reči
- apsorber kinetičke energije
- železnica
- elastoplastična deformacija
- kontakt
- analiza konačnim elementima (FEA)

Abstract

The paper describes the Finite Element Method (FEM) analysis of elastic plastic deformation of steel tube impact absorbers for railway vehicles. Experiment investigation is used as a basis for FEM modelling and simulation. The developed FEM model includes material nonlinearity (plasticity), nonlinear contact and large deformation of finite elements. All aspects used in the absorber FEM model are explained in detail. The finite element analysis results for a chosen absorber are presented and discussed. The developed model opens the possibilities for future investigations of similar problems.

Izvod

Rad daje opis analize elastoplastičnih deformacija čeličnog cevnog apsorbera kinetičke energije sudara železničkih vozila metodom konačnih elemenata (FEM). Eksperimentalna istraživanja korišćena su kao osnova za modeliranje i simulaciju FEM modela. Razvijeni model konačnih elemenata uključuje nelinearne karakteristike materijala (plastičnost), nelinearni kontakt i velike deformacije konačnih elemenata. Svi aspekti korišćeni u FEM modelu apsorbera detaljno su opisani. Rezultati FEM analize za izabrani apsorber prikazani su i analizirani. Razvijeni model otvara nove mogućnosti za buduća istraživanja u sličnim problemima.

INTRODUCTION

It is to mention that in the complex problem of reliability and structural integrity of vehicles in operation, in addition to plastic deformation, the cracking should be considered in three different aspects: theoretical, numerical and experimental. In that sense, elastic-plastic transition represents an important topic being connected with ductility, toughness and cracking. One interesting approach to this problem can be found in /1, 2/. However, numerical methods can be helpful in theoretical analysis /3-5/, but for in-service behaviour of a structure, experimental proof of proper structural behaviour is decisive. Full-scale experimental model tests, as presented in /6/ or in /7/, need to be applied, again strongly supported by updated numerical analysis. A similar approach is also accepted in the analysis presented herein.

The main role of the energy absorber of the railway vehicle is absorption of collision kinetic energy by controlled deformation in order to protect the vehicle main structure. Different solutions for energy absorber constructions are developed and examined, /8-13/. Energy absorption characteristics of one absorber type are investigated in this work. This type of absorber consists of a thin-walled seamless tube and a conical mandrel. At the moment of impact, the kinetic energy is taken by the mandrel that expands the tube and thus absorbs part of the collision kinetic energy. The energy absorption is result of elastic-plastic deformation of the tube and friction between the mandrel and tube. The total absorbed energy depends on the material quality (the material should have a high capacity of plasticity), manufacturing quality, and applied design of the tube and mandrel.

An important problem in energy absorber investigations are expensive experimental tests. In accordance with the numerical methods (as the Finite Element Method – FEM), and enormous rise in computing power, the investigation and analysis of energy absorbers without expensive experimenting is possible, /8-11/. In the light of these facts, the finite element analysis of plastic deformation of the steel

tube kinetic energy absorber is performed and described here. The FEM model for the simulation of the investigated absorber type is developed in accordance with experimental results, and in detail described in /12, 13/.

ABSORBER SHAPE AND SIZE

The space available for a collision energy absorber, in an agreement with a standard European rail vehicle buffer, is the limiting factor for designing an absorption device. Dimensioning of absorption devices is performed according to installation point limitations (buffer dimensions and the frontal part of the main structure, and the collision energy absorber in the middle), the required amount of absorbed energy and experience in frontal rail vehicle collisions.

Details of the investigation are given in previous works, /12, 13/. The shape and dimensions of the elements chosen for research of steel tube absorbers of collision energy are given in Fig. 1. The mandrel is made of steel C45E (steel number 1.1191) /14, 15/, with a diameter of 90 mm and dimensions defined in Fig. 1. Tube elements are produced from standard seamless tubes of 1.0309 steel, 88.9 mm in diameter and 4 mm wall thickness.

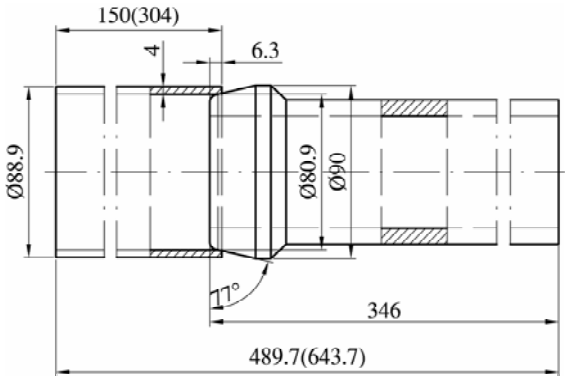

Figure 1. Absorber/mandrel shape and dimensions.
Slika 1. Oblik i dimenzije apsorbera/utiskivača

DETAILED DESCRIPTION OF FEA

Finite element model

The finite element method is used for stress-strain calculation of tube absorber. Commercial software ANSYS 11.0 is selected for the expansion process simulation. The finite element model is developed with axisymmetric planar finite elements defined by four nodes having two degrees of freedom at each node: translations in nodal x and y directions, Fig. 2.

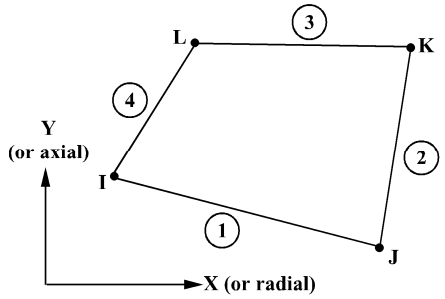

Figure 2. Planar finite elements used for axisymmetric the model.
Slika 2. Ravanski konačni elementi za osnosimetrični model

The FEM model for the steel tube absorber of impact energy and the mandrel is shown in Fig. 3. The finite element mesh (consisted of 357 nodes and 358 elements) and defined boundary conditions are also illustrated. Boundary conditions are defined through the constrained displacement in x and y direction for tube end nodes, placed opposite of the mandrel. The mandrel displacement constrains are defined by contact of mandrel and the internal tube surface before the start of indentation.

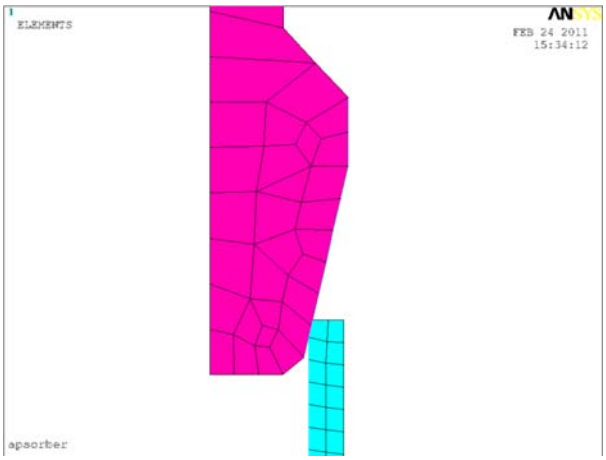

Figure 3. Tube absorber-mandrel FME model.
Slika 3. FME model cevnog apsorbera-utiskivača

Nonlinear contact definition

Surface-to-surface contact elements are chosen for simulation of contact conditions between internal surface of tube absorber and mandrel conical surface.

The surface-to-surface contact elements have several advantages over the node-to-node element, /16/.

Support lower and higher order elements on the contact and target that provide better contact results needed for typical engineering purposes, such as normal pressure and friction stress contour plots, have no restrictions on the shape of the target surface, /7/. Surface discontinuities can be physical or due to mesh discretization. The penalty method contact algorithm is used in finite element calculations, /16, 17/. The friction coefficient $\mu = 0.19$ is defined for contact surfaces, /10, 12/.

Figure 4. Contact elements and normals on contact elements
Slika 4. Kontaktni elementi i normale kontaktnih elemenata

Figure 4 presents defined contact elements for the investigated contact pair. In the model, initial penetration in contact is defined and the programme option for automatic contact adjustment (limit penetration) is chosen. With this procedure, the boundary condition for the mandrel may be defined as described in the previous part of this paper.

Material nonlinearity definition

Material nonlinearities occur because of the nonlinear relationship between stress and strain, that is, the stress is a nonlinear function of strain. The relationship is path-dependent so that the stress depends on the strain history as well as on the strain itself. Rate-independent plasticity is characterised by the irreversible instantaneous straining that occurs in a material. The definition of elastic strain for the case of nonlinear materials has the form:

$$\left\{\varepsilon^{el}\right\}=\left\{\varepsilon\right\}-\left\{\varepsilon^{th}\right\}-\left\{\varepsilon^{pl}\right\}-\left\{\varepsilon^{cr}\right\}-\left\{\varepsilon^{sw}\right\} \quad (1)$$

where: ε^{el} – elastic strain vector; ε – total strain vector; ε^{th} – thermal strain vector; ε^{pl} – plastic strain vector; ε^{cr} – creep strain vector; ε^{sw} – swelling strain vector.

In this case, $\{\varepsilon\}$ is the strain measured by a strain gauge. Equation (1) is only involved to show the relationships between the terms.

In finite element postprocessing, the total strain is reported as:

$$\left\{\varepsilon^{tot}\right\}=\left\{\varepsilon^{el}\right\}+\left\{\varepsilon^{pl}\right\}+\left\{\varepsilon^{cr}\right\} \quad (2)$$

where: ε^{tot} – component of total strain.

Comparing the last two equations,

$$\left\{\varepsilon^{tot}\right\}=\left\{\varepsilon\right\}-\left\{\varepsilon^{th}\right\}-\left\{\varepsilon^{sw}\right\} \quad (3)$$

The difference between these two "total" strains stems from the different usages: $\{\varepsilon\}$ can be used to compare strain gauge results and ε^{tot} can be used to plot nonlinear stress-strain curves.

Plasticity

Most common engineering materials exhibit a linear stress-strain relationship up to a stress level known as the *proportional limit*. Beyond this limit, the stress-strain relationship will become nonlinear, but will not necessarily become inelastic. Plastic behaviour characterised by non-recoverable strain begins when stresses exceed the material's *yield point*. Because there is usually little difference between the yield point and the proportional limit, it could be assumed that these two points coincide in plasticity analyses, Fig. 5.

Plasticity is a non-conservative, path-dependent phenomenon. In other words, the sequence in which loads are applied and in which plastic responses occur affects the final results. For attainment of plastic response in analysis, loads should apply as a series of small incremental load steps or time steps, so that the model will follow the load-response path as closely as possible.

Other kinds of nonlinear behaviour might also occur along with plasticity. In particular, large deflection and large strain geometric nonlinearities will often be associated with plastic material response.

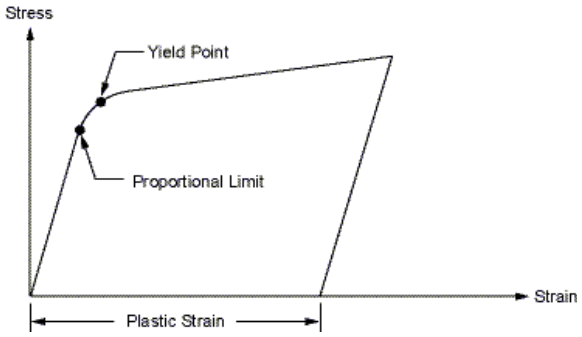

Figure 5. Elastic-plastic stresss-strain curve.
Slika 5. Elastoplastična karakteristika napon-deformacija

For efficient modelling nonlinear material characteristic with plasticity, the plasticity theory provides a mathematical relationship that characterises the elastic-plastic response of materials. There are three components in the rate-independent plasticity theory: the yield criterion; flow rule; and the hardening rule.

The *yield criterion* determines the stress level at which yielding is initiated. For multi-component stresses, this is represented as a function of the individual components, $f(\{\sigma\})$, which can be interpreted as an equivalent stress σ_e:

$$\sigma_e = f\left(\left\{\sigma\right\}\right) \quad (4)$$

where: $\{\sigma\}$ – stress vector.

When the equivalent stress is equal to a material yield parameter σ_y, the material will develop plastic strains. If σ_e is less than σ_y:

$$f\left(\left\{\sigma\right\}\right)=\sigma_y \quad (5)$$

the material is elastic and the stresses will develop according to elastic stress-strain relations. Note that the equivalent stress can never exceed the material yield stress since in this case plastic strains would develop instantaneously, thereby reducing the stress to the material yield.

The flow rule determines the direction of plastic straining and is given as:

$$\left\{d\varepsilon^{pl}\right\}=\lambda\left\{\frac{\partial Q}{\partial \sigma}\right\} \quad (6)$$

where: λ – plastic strain increment (which determines the amount of plastic straining); Q – function of stress termed the plastic potential (which determines the direction of plastic straining).

If Q is the yield function (as is normally assumed), the flow rule is termed associative and the plastic strains occur in a direction normal to the yield surface. The hardening rule describes the changing of the yield surface with progressive yielding, so that the conditions (i.e. stress states) for subsequent yielding can be established. Two hardening rules are available: work (or isotropic) hardening and kinematic hardening. In work hardening, the yield surface remains centred about its initial centreline and expands in size as plastic strains develop. For materials with isotropic plastic behaviour this is termed isotropic hardening and is shown in Fig. 6a. Kinematic hardening assumes that the yield surface remains constant in size and the surface translates in stress space with progressive yielding, as shown in Fig. 6b.

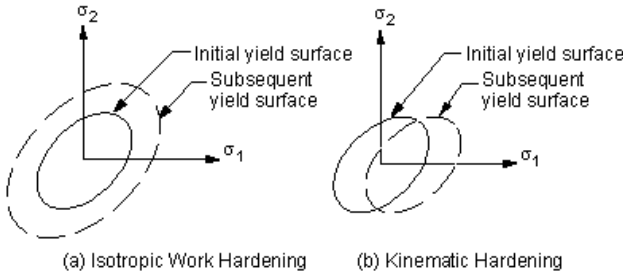

Figure 6. Types of hardening rules.
Slika 6. Tipovi ojačavanja

If the equivalent stress computed using elastic properties exceeds the material yield, then plastic straining must occur. Plastic strains reduce the stress in order to satisfy the yield criterion, (Eq.(5)). Based on the theory previously presented in the section, the plastic strain increment is readily calculated.

The hardening rule states that the yield criterion changes with work hardening and/or with kinematic hardening. Incorporating these dependencies into Eq.(5), and recasting it into the following form:

$$F\left(\{\sigma\},k,\{\alpha\}\right)=0 \tag{7}$$

where: k – plastic work; $\{\alpha\}$ – translation of yield surface; k and $\{\alpha\}$ are termed internal or state variables.

Specifically, the plastic work is the sum of the plastic work done over the history of loading:

$$k=\int\{\sigma\}^T[M]\left\{d\varepsilon^{pl}\right\} \tag{8}$$

where:

$$[M]=\begin{bmatrix}1&0&0&0&0&0\\0&1&0&0&0&0\\0&0&1&0&0&0\\0&0&0&2&0&0\\0&0&0&0&2&0\\0&0&0&0&0&2\end{bmatrix}$$

and translation (or shift) of the yield surface is also history dependent and is given as:

$$\{\alpha\}=\int C\left\{d\varepsilon^{pl}\right\} \tag{9}$$

where: C – material parameter; $\{\alpha\}$ – back stress (location of the centre of the yield surface).

Eq.(7) can be differentiated so that the consistency condition is:

$$dF=\left\{\frac{\partial F}{\partial\sigma}\right\}^T[M]\{d\sigma\}+\frac{\partial F}{\partial k}dk+\left\{\frac{\partial F}{\partial\alpha}\right\}^T[M]\{d\alpha\}=0 \tag{10}$$

Noting from Eq.(8) that:

$$dk=\{\sigma\}^T[M]\left\{d\varepsilon^{pl}\right\} \tag{11}$$

and from Eq.(9) that:

$$\{d\alpha\}=C\left\{d\varepsilon^{pl}\right\} \tag{12}$$

Eq.(10) becomes:

$$\left\{\frac{\partial F}{\partial\sigma}\right\}^T[M]\{d\sigma\}+\frac{\partial F}{\partial k}\{\sigma\}^T[M]\left\{d\varepsilon^{pl}\right\}+ +C\left\{\frac{\partial F}{\partial\alpha}\right\}^T[M]\left\{d\varepsilon^{pl}\right\}=0 \tag{13}$$

The stress increment can be computed via the elastic stress-strain relations:

$$\{d\sigma\}=[D]\left\{d\varepsilon^{el}\right\} \tag{14}$$

where: $[D]$ – stress-strain matrix, with

$$\left\{d\varepsilon^{el}\right\}=\{d\varepsilon\}-\left\{d\varepsilon^{pl}\right\} \tag{15}$$

since the total strain increment can be divided into an elastic and plastic part.

Substituting Eq.(6) into Eqs.(13) and (15) and combining Eqs.(13), (14) and (15) yields:

$$\lambda=\frac{\left\{\frac{\partial F}{\partial\sigma}\right\}^T[M][D]\{d\varepsilon\}}{-\left\{\frac{\partial F}{\partial k}\right\}\{\sigma\}^T[M]\left\{\frac{\partial Q}{\partial\sigma}\right\}-C\left\{\frac{\partial F}{\partial\alpha}\right\}^T[M]\left\{\frac{\partial Q}{\partial\sigma}\right\}+\left\{\frac{\partial F}{\partial\sigma}\right\}^T[M][D]\left\{\frac{\partial Q}{\partial\sigma}\right\}} \tag{16}$$

The size of the plastic strain increment is therefore related to the total increment in strain, the current stress state, and the specific forms of the yield and potential surfaces. The plastic strain increment is then computed using Eq.(6):

$$\left\{d\varepsilon^{pl}\right\}=\lambda\left\{\frac{\partial Q}{\partial\sigma}\right\} \tag{17}$$

Implementation

An Euler backward scheme is used to enforce the consistency condition Eq.(10). This ensures that the updated stress, strains, and internal variables are on the yield surface. The algorithm proceeds as follows:

1. The material value of σ_y (Eq.(5)) is determined for this time step (e.g. the yield stress at the current temperature).
2. The stresses are computed based on the trial strain $\{\varepsilon^{tr}\}$, which is the total strain minus the plastic strain from the previous time point (thermal and other effects are ignored):

$$\left\{\varepsilon_n^{tr}\right\}=\{\varepsilon_n\}-\left\{\varepsilon_{n-1}^{pl}\right\} \tag{18}$$

Notation and subscripts refer to the time point. Where all terms refer to the current time point, the subscript is dropped. The trial stress is then:

$$\left\{\sigma^{tr}\right\}=[D]\left\{\varepsilon^{tr}\right\} \tag{19}$$

3. The equivalent stress σ_e is evaluated at this stress level by Eq.(4). If σ_e is less than σ_y the material is elastic and no plastic strain increment is computed.
4. If the stress exceeds the material yield, the plastic multiplier λ is determined by a local Newton-Raphson iteration procedure, /18/.
5. $\{\Delta\varepsilon^{pl}\}$ is computed via Eq.(17).
6. The current plastic strain is updated:

$$\left\{\varepsilon_n^{pl}\right\}=\left\{\varepsilon_{n-1}^{pl}\right\}+\left\{\Delta\varepsilon^{pl}\right\} \tag{20}$$

where: $\{\varepsilon_n^{pl}\}$ – current plastic strains, and the elastic strain computed:

$$\{\varepsilon^{el}\} = \{\varepsilon^{tr}\} - \{\Delta\varepsilon^{pl}\} \tag{21}$$

where: ε^{el} – elastic strains.

The stress vector is:

$$\{\sigma\} = [D]\{\varepsilon^{el}\} \tag{22}$$

where: $\{\sigma\}$ – stresses.

7. The increments in the plastic work Δk and the centre of the yield surface $\{\Delta\alpha\}$ are computed via Eqs.(11) and (12), and the current values updated:

$$k_n = k_{n-1} + \Delta k \tag{23}$$

and

$$\{\alpha_n\} = \{\alpha_{n-1}\} + \{\Delta\alpha\} \tag{24}$$

where the subscript $n-1$ refers to the values at the previous time point.

8. For output purposes, an equivalent plastic strain $\hat{\varepsilon}^{pl}$, equivalent plastic strain increment $\Delta\hat{\varepsilon}^{pl}$, equivalent stress parameter $\hat{\sigma}_e^{pl}$ and stress ratio N are computed. The stress ratio is given as:

$$N = \frac{\sigma_e}{\sigma_y} \tag{25}$$

where: σ_e is evaluated using the trial stress. N is therefore greater than or equal to one when yielding is occurring and less than one when the stress state is elastic.

The equivalent plastic strain increment is given as:

$$\Delta\hat{\varepsilon}^{pl} = \left(\frac{2}{3}\{\varepsilon^{pl}\}^T [M]\{\Delta\varepsilon^{pl}\}\right)^{1/2} \tag{26}$$

The equivalent plastic strain and equivalent stress parameters are developed for each option in the next sections.

Note that the Euler backward integration scheme in step 4 is the radial return algorithm /19/ for the Von Mises yield criterion.

Elastic plastic stress-strain matrix

The tangent or elastic plastic stress-strain matrix is derived from the local Newton-Raphson iteration scheme used in step 4 above, /18/. It is therefore the consistent (or algorithmic) tangent. If the flow rule is not associative ($F \neq Q$), then the tangent is asymmetric.

Specialization for bilinear kinematic hardening

For the definition of plastic material characteristics in the presented model, authors used bilinear kinematic hardening model. The Bilinear Kinematic Hardening (BKIN) option assumes the total stress range is equal to twice the yield stress, so that the Bauschinger effect is included, Figs. 7 and 8 illustrate a typical display of bilinear kinematic hardening properties for different temperatures.

This option uses the von Mises yield criterion with the associated flow rule and kinematic hardening.

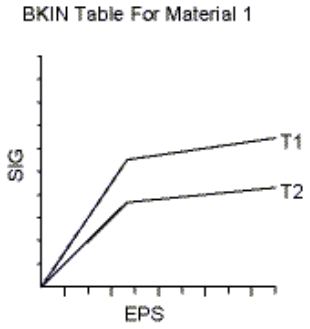

Figure 7. Bilinear kinematic hardening
Slika 7. Bilinearno kinematsko ojačavanje

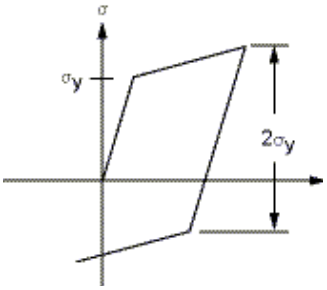

Figure 8. Bauschinger effect.
Slika 8. Baušingerov efekat

The equivalent stress (Eq.(4)) is therefore:

$$\sigma_e = \left[\frac{3}{2}(\{s\} - \{\alpha\})^T [M](\{s\} - \{\alpha\})\right]^{1/2} \tag{27}$$

where: $\{s\}$ – deviatoric stress vector:

$$\{s\} = \{\sigma\} - \sigma_m [1 \;\; 1 \;\; 1 \;\; 0 \;\; 0 \;\; 0]^T \tag{28}$$

where: σ_m – mean or hydrostatic stress = $\frac{1}{3}(\sigma_x + \sigma_y + \sigma_z)$; $\{\alpha\}$ – yield surface translation vector, (Eq.(12)).

Note that since Eq.(27) is dependent on the deviatoric stress, yielding is independent of the hydrostatic stress state. When σ_e is equal to uniaxial yield stress, σ_y, the material is assumed to yield. The yield criterion, Eq.(7) is therefore:

$$\Delta\hat{\varepsilon}^{pl} = \left(\frac{2}{3}\{\varepsilon^{pl}\}^T [M]\{\Delta\varepsilon^{pl}\}\right)^{1/2} \tag{29}$$

The associated flow rule yields:

$$\left\{\frac{\partial Q}{\partial\sigma}\right\} = \left\{\frac{\partial F}{\partial\sigma}\right\} = \frac{3}{2\sigma_e}(\{s\} - \{a\}) \tag{30}$$

so that the increment in plastic strain is normal to the yield surface. The associated flow rule with the Von Mises yield criterion is known as the Prandtl-Reuss flow equation.

The yield surface translation is defined as:

$$\{\alpha\} = 2G\{\varepsilon^{sh}\} \tag{31}$$

where: G – shear modulus = $E/(2(1+\nu))$; E – Young's modulus; ν – Poisson's ratio.

The shift strain is computed analogously to Eq.(24):

$$\{\varepsilon_n^{sh}\} = \{\varepsilon_{n-1}^{sh}\} + \{\Delta\varepsilon^{sh}\} \tag{32}$$

where:

$$\{\Delta\varepsilon^{sh}\} = \frac{C}{2G}\{\Delta\varepsilon^{pl}\},\ C = \frac{2}{3}\cdot\frac{EE_T}{E-E_T} \tag{33}$$

where: E – Young's modulus; and E_T – tangent modulus from the bilinear uniaxial stress-strain curve.

The yield surface translation $\{\varepsilon^{sh}\}$ is initially zero and changes with subsequent plastic straining. The equivalent plastic strain is dependent on the loading history and is defined to be:

$$\hat{\varepsilon}_n^{pl} = \hat{\varepsilon}_{n-1}^{pl} + \Delta\hat{\varepsilon}^{pl} \tag{34}$$

where: $\hat{\varepsilon}_n^{pl}$ – equivalent plastic strain for this time point; and $\hat{\varepsilon}_{n-1}^{pl}$ – equivalent plastic strain from the previous time point.

The equivalent stress parameter is defined to be:

$$\hat{\sigma}_e^{pl} = \sigma_y + \frac{EE_T}{E-E_T}\hat{\varepsilon}_n^{pl} \tag{35}$$

where: $\hat{\sigma}_e^{pl}$ – equivalent stress parameter.

Note that if there is no plastic straining ($\hat{\varepsilon}^{pl} = 0$), then $\hat{\sigma}_e^{pl}$ is equal to the yield stress. $\hat{\sigma}_e^{pl}$ only has meaning during the initial, monotonically increasing portion of the load history. If the load were to be reversed after plastic loading, the stresses and therefore σ_e would fall below yield but $\hat{\sigma}_e^{pl}$ would register above yield (since $\hat{\varepsilon}^{pl}$ is nonzero).

The stress and strain analysis for the tube apsorber is performed with elastic-plastic material characteristics presented in Fig. 9. Material characteristics are the same as used in the experimental investigation, /12/.

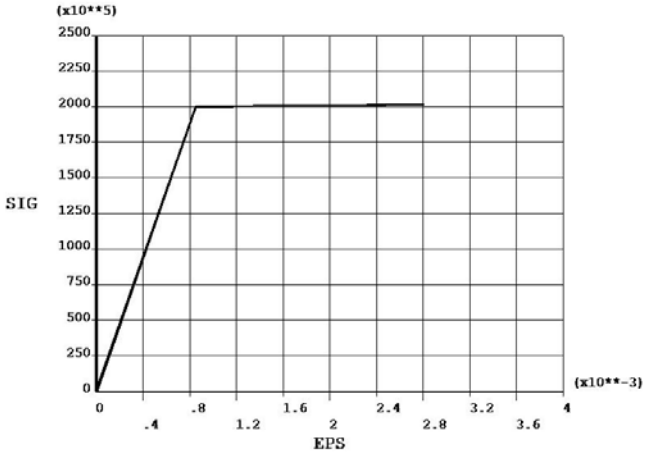

Figure 9. Bilinear kinematic hardening characteristic for the tube absorber material.
Slika 9. Karakteristika bilinearnog kinematskog ojačavanja za materijal cevnog apsorbera

External loads definition

External loads in finite element analysis are defined in accordance with the performed experiment, and discussed in detail in the previous part of this paper. Therefore, the displacement of the mandrel of 130 mm in 85 substeps is defined in the *y* direction.

Finite element analysis results

Finite element calculation is performed in 85 substeps with 726 cumulative iterations that made possible the contact conditions of convergence and strain-stress calculation. Figure 10 presents deformed and undeformed shape of the tube absorber and the mandrel at the last moment of the expansion process.

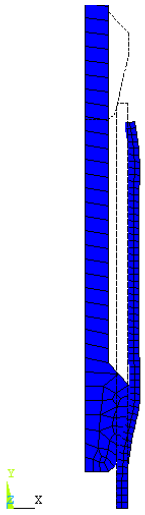

Figure 10. Deformed and undeformed shape of tube.
Slika 10. Deformisani i nedeformisani oblik cevi

Contour results for equivalent stresses at the last moment of tube expansion are shown in Fig. 11. Figure 12 presents normal stresses in the contact zone at the last moment of deformation process. Analysis of presented stress states allows us to conclude that expected results are obtained and that the developed FEM model could be recognised as a very good numerical simulation of the investigated problem.

For a comparative analysis of experiment and numerical results, Fig. 13a shows the total Von Mises deformation of the tube absorber, Fig. 13b shows elastic component of total deformation and Fig. 13c shows the plastic component of the total deformation. Comparative quantities of tube deformations (in percent) obtained during the experiment and FEM calculation are given in Table 1.

Table 1. Dimension variation due to expansion.
Tabela 1. Promena dimenzija kao rezultat proširivanja

Measured value	by Experiment (%)	by FEM (%)
Expansion	10.78	12.37
Tube wall thickness reduction	5.22	5.2875
Shortening	6.0	5.741

On the basis of the presented data, it is calculated that the plastic component of total deformation in the most distorted zone of tube absorber is approximately 94% of the total deformation.

Figure 14 represents the variation of the tube form during energy absorption and can be observed as a review of the variation of plastic deformation work/volume during the tube expansion process. Also, a 3D view of the tube form at the end of energy absorption is given, Fig. 15.

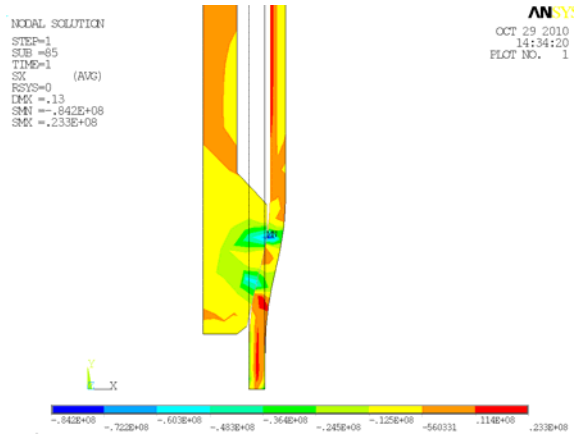

Figure 11. Contact stresses (N/m^2)
Slika 11. Kontaktni naponi (N/m^2)

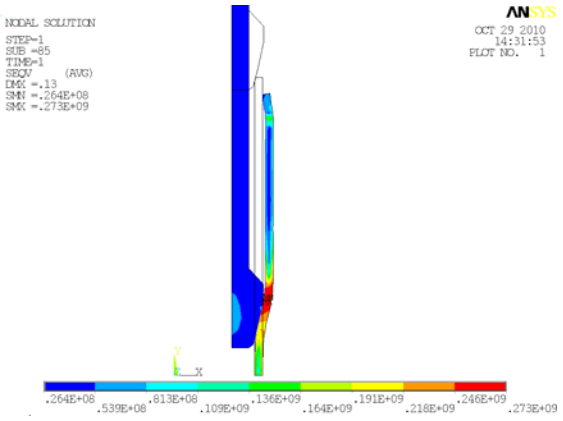

Figure 12. Von Mises equivalent stresses (N/m^2).
Slika 12. Von Mizesovi ekvivalentni naponi (N/m^2)

(a)

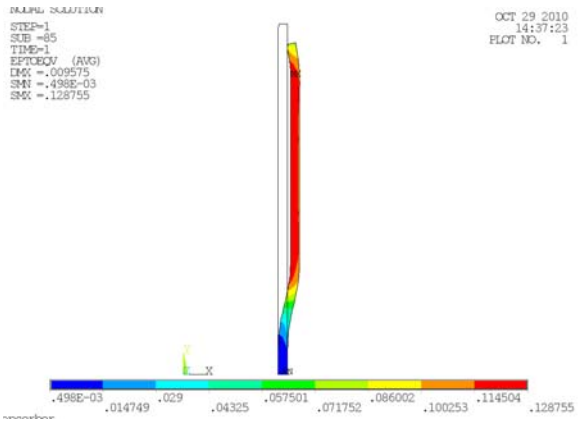

(b)

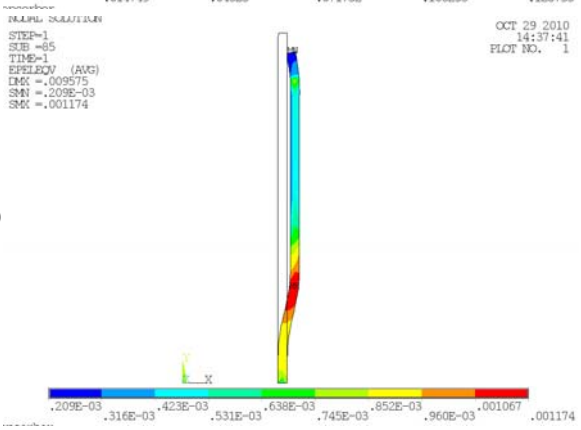

(c)

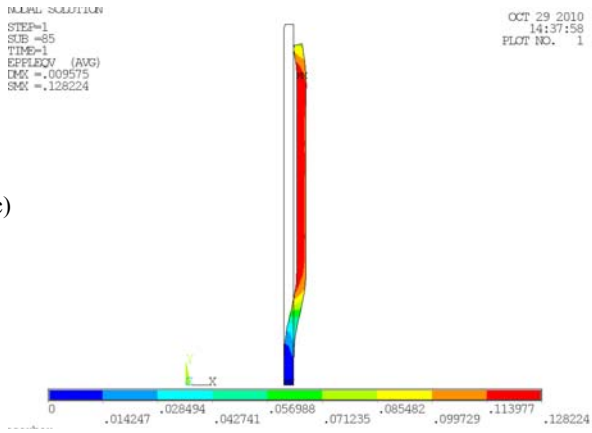

Figure 13. Von Mises tube deformations (N/m^2).
Slika 13. Von Misezove deformacije cevi (N/m^2)

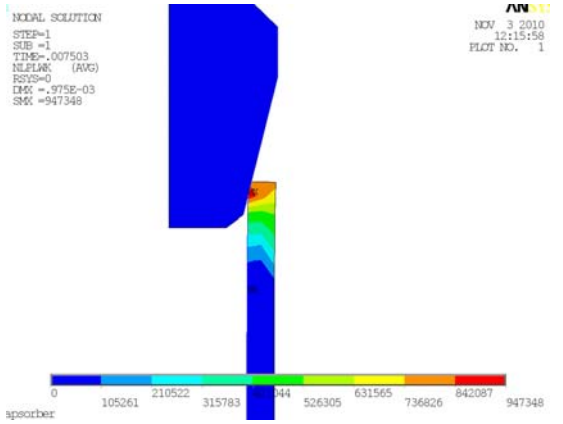

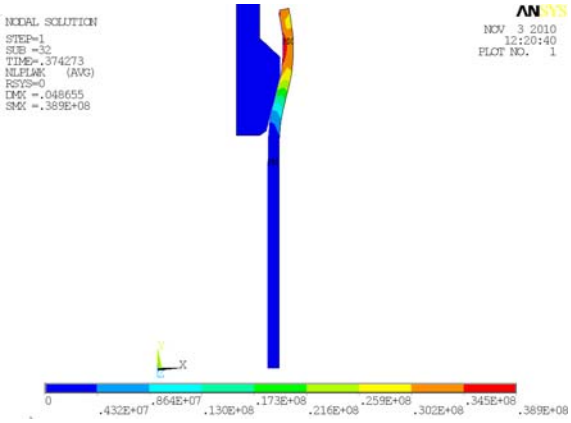

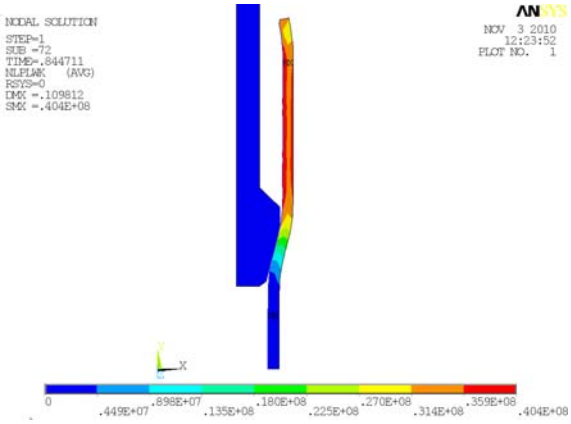

Figure 14. Plastic work/volume during tube expansion (J/m^3).
Slika 14. Rad plastične deformacije u toku proširivanja cevi (J/m^3)

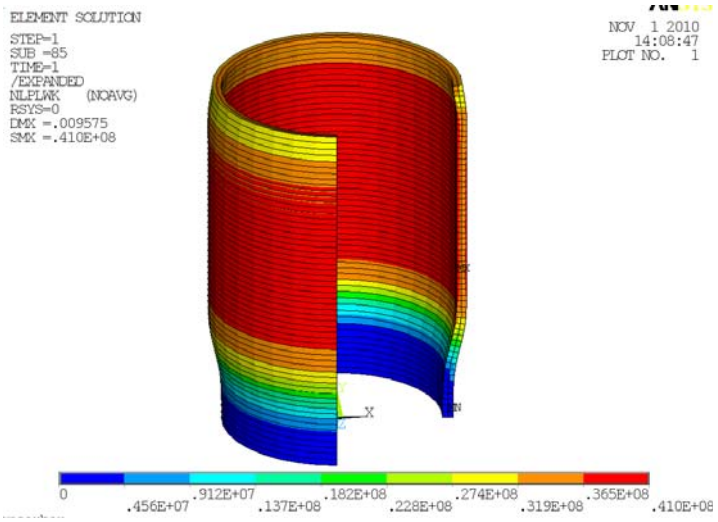

Figure 15. Plastic deformation work/volume at the end of deformation process (J/m^3).
Slika 15. Rad plastične deformacije/zapremina na kraju procesa deformisanja (J/m^3)

CONCLUSIONS

The investigation of plastic deformation work of steel tube energy absorber of railway vehicle impact described in this paper results in developing the finite element model for simulating experimental conditions. It is important to note that material characteristics modelling is one of the most significant of factors for plastic deformation simulation. Material nonlinearity definition used in the described model has given results in compliance with experimental results.

The developed FEM model simultaneously includes material nonlinearities (plasticity), nonlinear contact and large deformation. Comparison of FEM results for plastic deformation of tube during expansion and tube absorber deformation during testing exhibited excellent agreement.

With the aspect of very expensive experimental testing and investigation of tube energy absorbers of railway vehicle impact, the presented numerical simulation offers the way how to analyse and design railway absorbers and also enables further optimizing of shock absorbers.

ACKNOWLEDGEMENTS

Parts of this research are supported by the Ministry of Education and Science of the Republic of Serbia Grant OI 174001 Dynamics of hybrid systems with complex structures, Mechanics of materials.

REFERENCES

1. Pankaj, T., *Elastic-plastic transition stresses in an isotropic disc having variable thickness subjected to internal pressure*, Struc. Int. and Life (2008), Vol.9, No2, pp.125-132.
2. Pankaj, T., *Elastic-plastic transition in a thin rotating disc having variable density with inclusion*, Struc. Int. and Life, (2008), Vol.9, No3, pp.171-180.
3. Berković, M., *Numerical Methods in Fracture Mechanics*, Struc. Int. and Life, (2004), Vol.4, No2, pp.63-66.
4. Berković, M., *Problems of Plane and Triaxial Stress States in Pressure Vessels and Pipelines*, Struc. Int. and Life, (2004), Vol.4, No2, pp.67-74.
5. Popović, A., Marković, M., Panić, B., Nikolić, M., *Data Acquisition and Processing*, Struc. Int. and Life (2006), Vol.6, No1-2, pp.53-64.
6. Maneski, T., Milošević-Mitić, V., *Numerical and experimental diagnostics of structural strength*, Struc. Int. and Life, (2010), Vol.10, No1, pp.3-10.
7. Maksimović, S., Ilić, I., *Strength analysis of mechanically fastened joints on composite plate*, Struc. Int. and Life (2006), Vol.6, No1-2, pp.23-30.
8. Zhang, X., Cheng, G., Zhang, H., *Numerical investigations on a new type of energy-absorbing structure based on free inversion of tubes*, International Journal of Mechanical Sciences (2009) vol.51, pp.64-76.
9. Yang, J., Luo, M., Hua, Y., Lu, G., *Energy absorption of expansion tubes using a conical–cylindrical die: Experiments and numerical simulation*, International Journal of Mechanical Sciences (2010) vol.52, pp.716-725.
10. Boiko, A., *Energy absorption optimization of multiaction plastic working element of vehicle systems under emergency impact loading conditions*, Strength of Materials (2002) Vol.34, No.3, pp.305-309.
11. Schaeffer, L., Brito, A., *FEM Numerical Simulation and Experimental Investigation on End-Forming of Thin-Walled Tubes Using a Die*, Steel Research Int., (2007), vol.78, No.10-11, pp.798-803.
12. Krivokapić, M., Research of the Characteristics of the Collision Kinematic Energy Tube Absorber at the Railway Vehicles, MSc Thesis (in Serbian), (2005), University of Belgrade, Faculty of Mechanical Engineering, Belgrade, Serbia.
13. Simić, G., et al., *Experimental research of characteristics of shock absorbers of impact energy of passenger coaches*, Experimental techniques, July/August 2009, (2009), pp.29-35.
14. EN 10027-1:2005, Designation systems for steels-Part 1: Steel names (2005).
15. EN 10027-2:1992, Designation systems for steels-Part 2: Steel numbers (1992).
16. The ANSYS User's Manual, Theory, Release 11.0 (2008).
17. Vulović, S., Živković, M., Grujović, N., *Contact Problems Based on the Penalty Method,* Scientific Technical Review (2008), vol.58, No.3-4, pp.33-37.
18. Simo, J.C., Taylor, R.L., *Consistent Tangent Operators for Rate-Independent Elastoplasticity*, Computer Methods in Applied Mechanics and Engineering, (1985), vol.48, pp.101-118.
19. Krieg, R.D., Krieg, D.B., *Accuracies of Numerical Solution Methods for the Elastic-Perfectly Plastic Model*, Journal of Pressure Vessel Technology, (1977)., vol.99, No.4, Series J, Transactions of the ASME, November, pp.510-515.